IJASS
International Journal of
Aeronautical and Space Sciences

Development of Flight Control System and Troubleshooting on Flight Test of a Tilt-Rotor Unmanned Aerial Vehicle

Youngshin Kang*, Bum-Jin Park**, Am Cho***, Chang-Sun Yoo**** and Sam-Ok Koo*****

Korea Aerospace Research Institute, Daejeon 34133, Republic of Korea

Min-Jea Tahk******

Korea Advanced Institute of Science and Technology, Daejeon 34141, Republic of Korea

Abstract

The full results of troubleshooting process related to the flight control system of a tilt-rotor type UAV in the flight tests are described. Flight tests were conducted in helicopter, conversion, and airplane modes. The vehicle was flown using automatic functions, which include speed-hold, altitude-hold, heading-hold, guidance modes, as well as automatic take-off and landing. Many unexpected problems occurred during the envelope expansion tests which were mostly under those automatic functions. The anomalies in helicopter mode include vortex ring state (VRS), long delay in the automatic take-off, and the initial overshoot in the automatic landing. In contrast, the anomalies in conversion mode are untrimmed AOS oscillation and the calibration errors of the air data sensors. The problems of low damping in rotor speed and roll rate responses are found in airplane mode. Once all of the known problems had been solved, the vehicle in airplane mode gradually reached the maximum design speed of 440km/h at the operation altitude of 3km. This paper also presents a comprehensive detailing of the control systems of the tilt-rotor unmanned air vehicle (UAV).

Key words: troubleshooting, tilt-rotor, flight test, flight control, vertical take-off and landing (VTOL)

1. Introduction

Smart unmanned air vehicle (UAV) is a tilt-rotor type aircraft that combines the ability to perform vertical take-off and landing while maintaining the ability to meet high speed cruise performance for the Korean civil UAV missions. These missions include coast guard, disaster detection, weather forecasting, and environmental monitoring, etc. It reaches the maximum design speed of V_{TAS} 440km/h at an altitude of 3km [1, 2]. A snapshot of the flight test in airplane mode of the Smart UAV is shown in Fig. 1.

In the initial phase of the Smart UAV program, a trade-off was conducted among many VTOL configurations, and the tilt-rotor type achieved the best results in terms of performance for the civil missions, especially at high speeds and high altitudes [3]. The development of the Smart UAV

was strongly inspired by Bell's TR-911X, the first UAV of this kind [4, 5]. The TR-911X was a 7/8 scaled demonstrator of

Fig. 1. Flight test in airplane mode of the Smart UAV [2]

(cc)
  * Principal Researcher, Future Aircraft Research Division, Ph. D, Corresponding author: kangys@kari.re.kr
 ** Senior Researcher, Future Aircraft Research Division, Ph. D.
 *** Senior Researcher, Future Aircraft Research Division, Ph. D.
 **** Principal Researcher, Future Aircraft Research Division, Ph. D.
 ***** Principal Researcher, Future Aircraft Research Division, Ph. D.
 ****** Professor, Department of Aerospace Engineering, Ph.D.

the production model, TR-918 [6]. Most of the detailed troubleshooting on the flight test results of those unmanned and manned tilt-rotor aircraft [7, 8] were undisclosed.

The basic specifications of the Smart UAV, TR-100, are compared with those of the TR-918 Eagle Eye in Table 1 [5, 6]. The Smart UAV is configured similarly to the benchmarked Eagle Eye. The remarkable difference between the Smart UAV and the Eagle Eye is the T-tail, which is intended to avoid immersion of the tail into the rotor wake under a low speed [4], and internal design. The maximum design speed of the TR-100 is much greater than that of the TR-918. However, the maximum payload of the latter is higher.

Before conducting the flight test of the full-scale Smart UAV, the control law of the tilt-rotor UAV was verified through fully autonomous flights of a 40% scaled model named TR-40 [9-11]. The control law was designed using the general tilt-rotor nonlinear simulation model based on NASA technical reports [12, 13]. The basic control surface mixers of the Smart UAV also followed the NASA reports in terms of modifications based on the flight test results of the TR-40 and Smart UAV.

Although the control law has been proven through the flight test of the TR-40 [11], many unexpected problems were still inevitable due to the differences in scale and engine type. The troubleshooting was conducted mostly in helicopter mode, the initial phase of flight test [14]. In this stage, the vehicle encountered vortex ring state (VRS), divergence in heading, large oscillation of vertical speed, and various sensor problems, etc. The VRS during the abrupt descent [14] will be revisited to explain the improvement of the control law on the heave axis. The other anomalies that

this study experienced in the helicopter mode were the long delay on the ground in automatic take-off and the initial overshoot when the automatic landing was engaged. The anomalies are found in conversion mode as well. They were the untrimmed AOS problem, which caused slow and large oscillation, and the calibration errors of air data sensors. Most of the problems related to autonomous functions were found and solved in the earlier phases, and the only issue that the airplane mode had was the low damping in rotor speed and roll rate response.

The contribution of this paper is listed as follows:

1) This paper presents the flight control system of the Smart UAV, its verification via the flight test, and the trouble-shooting data. They will establish a better understanding of the development and flight test of unconventional tilt-rotor UAV.

2) This paper elaborates on the flight control system and anomalies associated with it, which are found during the flight test of tilt-rotor type Smart UAV. The anomalies of any UAV have seldom been discussed in detail in the literature. The troubleshooting procedure shown in this paper may inspire readers and help them avoid anomalies of their own UAV and solve the problems when they encounter inevitable anomalies.

The organization of the paper is as follows: Section II provides a summary of the flight control system and control modes. Section III elaborates on the anomalies and solutions in helicopter, conversion, and airplane modes of flight test for the Smart UAV. The comparison of the flight envelops between the Smart UAV and Eagle Eye will be presented. The

Table 1. Specification of the Smart UAV and Eagle Eye

Parameters		TR-100 Smart UAV	TR-918 Eagle Eye [5,6]
Design gross weight (Kg)		1000	1179.3
Payload weight (Kg)		100	90-135
Wing span (m)		4	4.32
Length (m)		5	5.56
Height(m)		1.87	1.89
Rotor diameter (m)		2.864	3.05
Disc area per rotor (m^2)		6.44	7.30
Rotor speed (rpm)	in helicopter/conversion	1573 (98%)	1509* (100%)
	in airplane	1256 (82%)	1207* (80%)
Conversion Range (0° at airplane)		0-93°	0-95°
Maximum level flight speed (km/h)		440	370.4
Service ceiling(m)		6,000	6,096
Range (km)		200	185.2
Endurance (hrs)		> 5	> 6
Power Plant		PW 206C	PW207D
Maximum Power		550 HP	641 HP

* estimated value based on the tip speed of rotor

conclusion is presented in Section IV.

2. Control System Developments

2.1 Operation and Control Systems

The Smart UAV operation system consists of a ground control station (GCS), dual data-link system, and the tilt-rotor aircraft as illustrated in Fig. 2. The figure shows the primary components of the flight control system (FCS) as parts of the aircraft system. The FCS consists of the digital flight control computer (DFCC), GPS/INS sensor, radar altimeter, air data computer (ADC) connected with the nose boom sensor, and the actuator control unit (ACU) integrated with 13 electric actuators. The dual FCS architecture is designed to have a primary and backup structure. The backup channel is activated when the primary channel experiences any form of critical failure. The DFCC and ACU have cross-channel data links between the primary and backup channels, which makes the channels mutually accessible when obtaining the status, which includes the failure information and sensor data. Both of the DFCCs monitor the built-in test (BIT) signals of all the sensors and the ACU.

The GPS/INS sensor and its Novatel GPS receiver have dual redundancy. The GPS/INS is used not only as a navigation sensor but also as a backup for the estimation of calibrated airspeed (V_{CAS}), true airspeed (V_{TAS}), and the altitude in the case of ADC failure. The estimated air speed can be calculated as Eqs. (1) and (2).

$$V_{TAS}^{est} \approx \sqrt{\left(u^2 + v^2 + w^2\right)} \tag{1}$$

$$V_{CAS}^{est} = \sqrt{\frac{\rho}{\rho_0}} V_{TAS}^{est} \tag{2}$$

where ρ and ρ_0 are the air density at the altitude and seal level, respectively.

Although the radar altimeter and ADC have single redundancy as shown in Fig 2, the reliability of the single ADC is acceptable because it has a backup of GPS/INS sensors. The production type Smart UAV will be equipped with an upgraded dual DFCC, which contains the embedded dual ADC function. The radar altimeter is solely used for automatic landing and only determines the flare altitude where the descent rate fall below 1m/sec for smooth touch down. The failure of the radar altimeter is not fatal, because the failed radar altimeter is smoothly and automatically replaced by the GPS altitude. Once the radar altimeter fails, the flare altitude is determined using the difference between the specified touch down altitude and current GPS altitude. Because the height error of GPS sensor is critical, the flare altitude is set to be higher than the valid altitude from the radar altimeter. It is noteworthy that radar altimeter just measures the distance between the touch down point and the aircraft. Therefore, the DFCC should know the GPS altitude of the touch down point in order to determine the flare altitude in case of radar altimeter failure.

The dual ACUs control the dual channel electric actuators of which the controllers are newly developed because they are not available from the manufacturer [15]. The dual ACU controllers of the left and right rotors simultaneously manage all three actuators for collective, longitudinal, and lateral cyclic. The flaperon ACU and conversion ACU manage only the flaperon and the nacelle conversion actuator, respectively. The elevator actuator has a single channel because it requires only a small volume for installation. Therefore, the elevator surface is separated into left and right sides, where each consists of independent actuators for dual redundancy. The throttle actuator is also chosen to
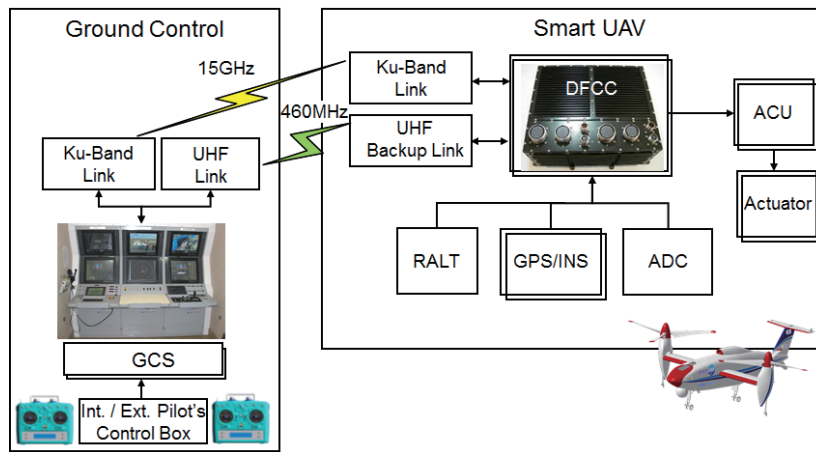

Fig. 2. Unmanned Aircraft Systems of Smart UAV

have single redundancy because its high level of reliability allows the possibility for the second channel to be removed. The production type will be upgraded with all dual channel actuators to gain a higher level of reliability.

The GCS provides the control function for both the external pilot (EP) and internal pilot (IP) as listed in Table 2. The EP can use only the external pilot box (PBX) for manual control while the IP can use both of the PBX and the pilot bay (PBY) inside the GCS for all the control interfaces including the knob control and guidance function as shown in the left side of Fig. 2.

2.2 Control Law Development

The most fundamental controller of the tilt-rotor aircraft is the control surface mixer because the pilot has only 4 stick commands, i.e. longitudinal, lateral, directional, and collective, to control 13 actuators, i.e. 6 for rotors, 2 for nacelles, 2 for flaperons, 2 for elevators, and 1 for the power lever. Therefore, the control surface mixer is designed to allocate the control stick commands to the actuators of the control surfaces according to the airspeed or nacelle tilt angle as shown in Fig. 3.

The initial control surface mixer of the Smart UAV is designed similarly to that of the Bell XV-15 [12] with the exception of the lateral cyclic and rudder. The XV-15 does not have the lateral cyclic control, i.e. 6th and 7th outputs of Fig. 3, and the Smart UAV does not have the rudder surface. The rudder is replaced with the 2deg. differential collective out of total 48deg., i.e. 8th and 9th outputs of Fig. 3, similar to that of Bell's Eagle Eye [4, 5]. The mixer for control surface can be

designed using control moment derivatives, i.e. the elements of B matrix of the linear model, to yield gradual increase according to the increase of speed [16]. This behavior is similar to a general fixed wing aircraft model.

The primary control modes of the Smart UAV is presented in Table 2. The attitude stability and control augmentation system (SCAS) is the basic augmented controller of the Smart UAV. The longitudinal and lateral stick controls generate the pitch and roll attitude commands, respectively. The directional stick generates the yaw rate command, which is combined with the sideslip (β) feedback. The heading-hold is engaged when the directional stick command is at neutral. The vertical stick generates the simple collective and throttle command with the vertical speed augmentation. The rate SCAS, named as SAS stick mode, can be used for manual mode in case of a failure of attitude and speed sensors.

In order to provide the EP with easier hover control using a longitudinal and lateral ground speed command, the GPS stick mode can be engaged by the IP when he or she pushes the button of the touch panel of the PBY. If the EP, who has the control authority, releases the stick into neutral center position then the aircraft keeps hovering at the current position. This scheme is similar to the inertial velocity mode of the Eagle Eye [4]. The vertical stick command generates the altitude rate command and maintains the altitude if the stick command is neutral.

The altitude, speed, heading, or roll hold modes can be engaged and controlled by the touch panel and knob dials of the PBY. In helicopter mode, where the nacelle tilt angle is greater than 80 degrees, the altitude is controlled

Table 2. Flight control modes of Smart UAV

Inter-face	Prio-rity	Control mode	Remark
EP/ IP's PBX	1	SAS Stick (Autopilot Off)	Rate and thrust command
	2	SCAS Stick (Autopilot On)	Attitude and vertical speed command
	4	GPS Stick	Ground speed command and position hold (V_{CAS}<100km/h)
PBY for IP	2	Return home	Loss of link
		Collision Avoid	Intruder distance<1km (ADS-B based)
	3	Airspeed hold	GPS speed hold for V_{GPS}<50 km/h
		Baro-altitude hold	GPS altitude hold for V_{GPS}<50 km/h
		Heading hold	Prior to roll hold
		Roll hold	Disengaged V_{GPS}<50 km/h
	4	Auto hover	Approach and Hover (V_{CAS}<100km/h)
		Auto take off	V_{GPS}<50 km/h
		Auto landing	V_{GPS}<50 km/h
		Point Turn	Fade out near hover speed
		Preprogrammed	Climb turn is available
		Camera Guide	Fade out near hover speed
		Auto recovery	Linked return home

by both the engine power and collective pitch, while the airspeed is controlled by the pitch attitude. The altitude and speed controls are replaced with the pitch attitude and power controls, respectively, in airplane mode [2, 4]. These automatic changes in control authority are scheduled according to airspeed. Therefore, the altitude and speed holds are engaged simultaneously when the IP pushes either the altitude or speed hold button. The heading hold generates turn coordination commands, which includes the roll attitude command and corresponding yaw rate command at a high speed of helicopter mode. The roll command generated by the heading hold mode fades out gradually at a low speed close to hover.

The guidance laws consist of auto-hover, auto-take-off [17, 18], auto-landing [17, 18], point turn [1, 18], pre-programmed [2, 17, 18], camera guide [19], auto-recovery [17], return home [17], and collision avoidance [20] as listed in Table 2, where a lower number indicates higher priority. Therefore, the return home and collision avoidance modes have priority over the other guidance modes. The SCAS stick mode and the emergent guidance modes are of the same level of priority. This is because if the SCAS stick mode is not activated, then the return home and collision avoidance modes cannot be engaged autonomously whereas SCAS

stick command is not controllable under the situation of link loss or collision avoidance.

The guidance controls follow the Line-Of-Sight (LOS) method [21]. The common structure of the LOS guidance law is applied to each of the helicopter, conversion, and airplane modes. The buttons for the guidance command are activated when the IP establishes the required navigation information using the map screen on the upper side of the PBY. When the IP pushes any button on the touch panel, the aircraft flies autonomously and follows the given flight path using the provided information.

3. Flight Test Results and Troubleshooting

Most flight tests were performed under the guidance law that was explained in Chapter 2, with the exception of the first flight and the low speed turn-around flight near the take-off and landing position of the initial phase.

3.1 Helicopter Mode

The flight test in helicopter mode of the Smart UAV consists of manual and autonomous modes by the EP and
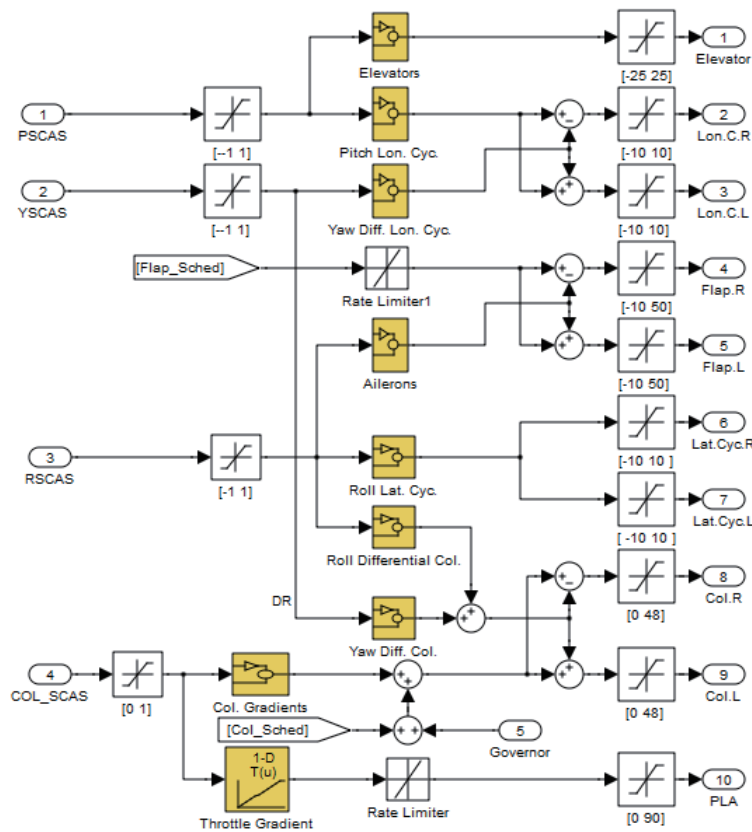

Fig. 3. Control surface mixer of Smart UAV

IP, respectively. The EP performed the manual take-offs and landings from hover, low-speed turns. The IP performed the same sorties using the autonomous function. The number of manual sorties was minimized due to the high workload of the EP, and most flights were performed by the IP. Because the autonomous take-off and landing functions were verified during the early phase of the flight test, all the subsequent flight test missions were performed using the autonomous functions in order to reduce the level of risk in the test [17, 18].

3.1.1 Recovery from Vortex Ring State (VRS)

The most dangerous situation throughout the whole flight test sorties of the Smart UAV occurred during the first automatic flight trial [14]. The aircraft climbed slowly under the altitude and speed hold mode as shown in Fig. 4 (a) when the IP took over the control from the EP and increased the speed while holding altitude at 140m. The climb rate was so small that nobody recognized it until the altitude reached 200m. As soon as the IP noticed it, he attempted to decrease the speed, trying to recover the altitude. However, his command was too excessive and resulted in the plunge

of the aircraft followed by a significant left roll due to the VRS as shown in the first plot of Fig. 4 (b). The descent rate reached about -500m/min, as shown in the third plot of Fig. 4 (b), before the EP abruptly took control using the "authority" switch of his PBX as shown in the first plot of Fig. 4 (b). Note that turning this switch enables the EP to override the whole control authority of the IP. The altitude rate feedback in the basic SCAS mode generated the maximum power command to recover the descent rate, and the rotor governor decreased the collective angle in order to reduce the surge in torque of the engine as shown in the second plot of Fig. 4 (b).

These automatic recovery procedures conducted by the SCAS controller and the EP barely saved the aircraft from the VRS by taking over the control authority from the IP. The reason for the unexpected climb was later found to be that the lower limit of the throttle command in the altitude hold controller was set higher than the required power. The lower limit was scheduled in terms of the tilt angle which began to decrease from a speed of 50km/h. Therefore, the altitude hold controller could not reduce the power to descend at around this speed of which the power required is much lower than that of hover as shown in Fig. 4 (c).

The architecture of the altitude hold mode was modified
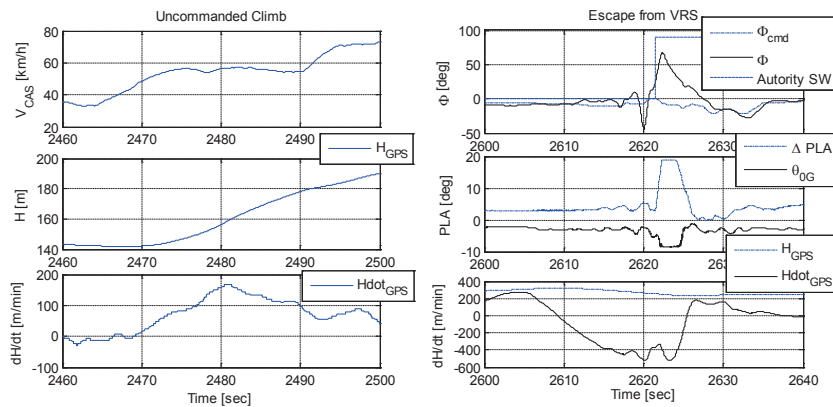
(a) Slow ascending due to the limit error

(b) Escape from vortex ring state by SCAS
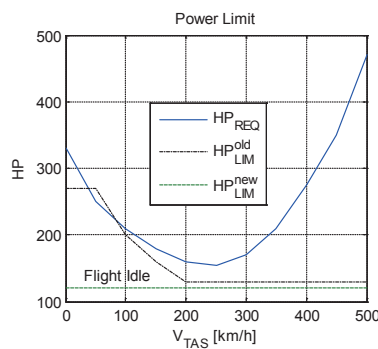
(c) Reduced power limit to flight idle

Fig. 4. Entry into and recovery from the vortex ring state [14]

from the altitude error command with the altitude rate damper to the altitude rate error command system of Eqs. (3) and (4) [16].

$$\delta_{COL} = \left(K_{dh} + \frac{K_{dh_i}}{s} \right) \cdot \left(\dot{h}_{cmd} - \dot{h} \right)$$ (3)

where

$$\dot{h}_{cmd} = K_h \left(h_{cmd} - h \right)$$ (4)

In addition, the lower limit of the throttle command of the altitude hold mode was brought down to the flight idle power as shown in Fig. 4(c). This means that the altitude hold mode has the full authority throughout the flight envelopes. The instability of engine operation under low power conditions can be prevented by applying the altitude rate limit (= -1.5 m/sec) which is chosen to avoid VRS during the descent in helicopter mode.

3.1.2 Long Delay in Automatic Take-off

At the initial phase of the automatic flight test, the aircraft could not instantly follow the take-off command from the IP, instead it delayed approximately 5 seconds as shown in the second plot of Fig. 5 (a).

In order to decrease the time delay on the ground for the automatic take-off, an initial value of the integrator in collective control of Eq. (3) is added when it was engaged by the amount of hover power. As a result, the time delay was decreased to less than 1.8 second as shown in the second plot of Fig. 5 (b). Further reduction in delay could not be achieved due to the rate limiter of the power lever actuator as shown in 10th output path of Fig. 3.

Note that the ground altitudes in the first plots of Fig. 5 (a) and (b) exhibit significant difference because they have distinct references of GPS altitude; the former and the latter were based on the (WGS 84) ellipsoid and the geoid (relative to the mean sea level) [22], respectively.

3.1.3 Initial Climb in Automatic Landing

During the first automatic landing trial, the aircraft climbed up for few seconds, and started descent for touch down as shown in the second plot of Fig. 6 (a). Although this problem was not critical or dangerous, it was not easy to solve in the initial phase of the helicopter flight test. The root cause of this problem was identified that the complicatedly entangled sequence of the altitude hold decision logics lost one frame of altitude hold mode when the IP engaged the automatic landing. The altitude hold mode should not be disengaged for any changes of autonomous control mode during the automatic flight. The altitude hold mode was set prior to the determination of automatic take-off and landing. Therefore, if the IP engaged the automatic take-off or landing, the altitude hold mode was disengaged within 1 frame (= 0.02sec) before the engagement. This caused an instant shift and return of the throttle command between the vertical stick command of PBX and altitude hold command. However, this anomaly did not affect the automatic take-off because of the time delay in the initial climb. This problem was fixed with the change of the sequence to determine the altitude hold mode at the last decision logic. The improved result was shown in Fig. 6 (b).

3.2 Conversion Mode

The flight test in conversion mode consists of flights under the speed, altitude and heading or roll hold modes for every 10deg. tilt angles from 80deg. (= helicopter mode) to 0deg. (=airplane mode). The acceleration and deceleration, climb and descent, left and right turns were performed at the same tilt angle interval. [23]
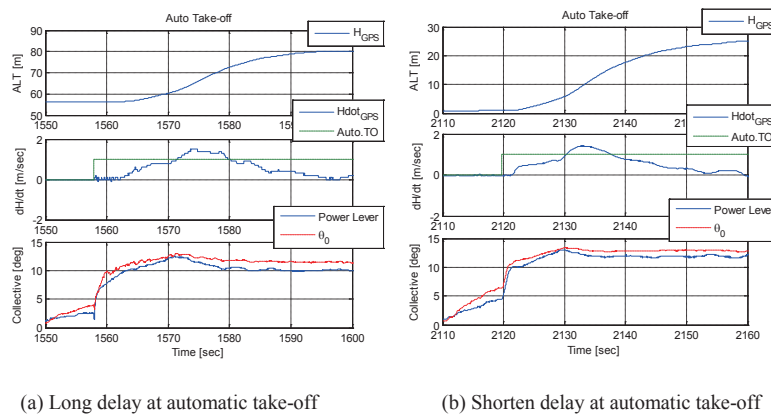

(a) Long delay at automatic take-off (b) Shorten delay at automatic take-off

Fig. 5. Improvement of the automatic take-off

126

3.2.1 Large Sideslip Oscillation

During the conversion tests in the envelop expansion, the slow and large angles of sideslip (AOS) oscillations occurred around a tilt angle of 75deg. The attempt to reduce the AOS oscillation through the yaw control, which increases the differential longitudinal cyclic pitch (i.e. δ_{B1}), was not effective because of the hysteresis phenomenon that is shown in Fig. 7 (a). The integrator component of the AOS feedback in the yaw axis failed to trim out the AOS because of the increase in δ_{B1} (i.e. pushed heading to the left) to reduce negative AOS resulted in excessive heading overshoot to a large positive AOS, and vice versa. Therefore, the additional vertical fins were attached to the tips of the horizontal tail as shown in Fig. 7 (b).

Although the original vertical tail is only half the size of the horizontal tail, the wind tunnel test verified that it provides sufficient directional stability. Therefore, the size of the vertical tail remained unchanged until the flight demonstration which revealed its poor performance. The additional vertical fins resolved the AOS hysteresis issues without any side effects. The full conversion test was completed in two sorties of flights after the vertical tail modification.

3.2.2 Calibration Errors in True Air Speed

The true airspeed are calibrated from the commercial air data system through the flight test results as shown in Fig. 8 (a)-(b). The errors in airspeed and barometric altitude result mostly from the pressure measurement error of pitot-static tube due to its installation configuration [24, 25]. By comparing the measured true airspeed (V_{TAS}) with the estimated V_{TAS} from the GPS ground velocity, the dynamic pressure error was identified to be about 16.08% of measured impact pressure (q_c) as shown in Fig. 8 (a). The impact pressure error (Δq) was measured in constant bank turns at the airspeeds of 110, 150, 190, and 250km/h. The measurement was taken twice at speed of 150 and 250km/h, because of the node points of nacelle conversion schedule at 70deg. and 0deg. The error of impact pressure, Δq, was fitted by the least square method as expressed in Eq. (5).
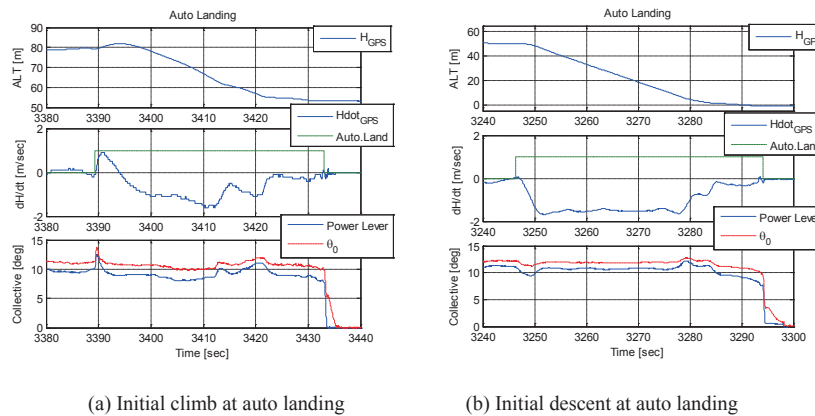
$$\Delta q \approx 0.1608 \times q_c \tag{5}$$

(a) Initial climb at auto landing   (b) Initial descent at auto landing

Fig. 6. Improvement of the automatic landing

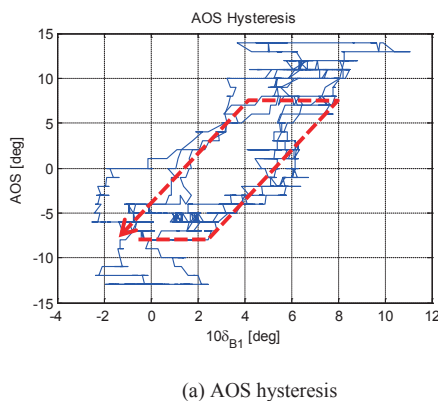(a) AOS hysteresis   (b) Vertical fin extensions

Fig. 7. Vertical fins on the outside of horizontal tail to overcome AOS hysteresis

As a result, the corrected V_{TAS} is calibrated as Eq. (6) and shown in Fig. 8 (b).

$$V_{TAS}^{cal} = \sqrt{1.1608} \times V_{TAS} \tag{6}$$
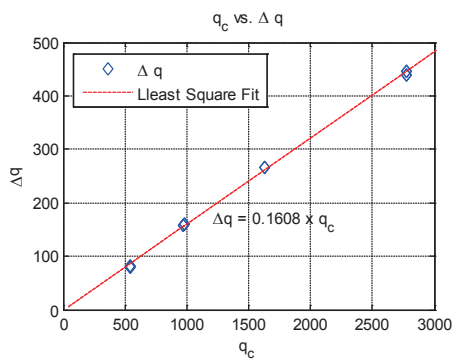
3.3 Airplane Mode

No critical problems in handling qualities occurred during the flight tests in airplane mode. This was because the fidelity of nonlinear dynamic model was high enough to design an accurate control law of Smart UAV [13]. The only issues were the tendencies of low damping in rotor speed and roll rate responses.

3.3.1 Rotor RPM Oscillation

A noteworthy tendency of TR-100 was the oscillation of rotor speed in the airplane mode as shown in Fig. 9 (a). The maximum overshoot of the RPM in airplane mode was approximately ±2%, which caused distinctive rotor noise. One of the root causes was that the collective angle was scheduled by airspeed in order to reduce the amount of output in the integrator controller of the rotor governor [12]. When the rotor speed increased, the collective (θ_0) also increased due to the rotor governor (θ_{0G}), which increased the airspeed (V_{CAS}) and the scheduled collective as well. Consequently, the rotor speed dropped back due to the excessive collective, and vice versa, as shown in Fig. 9 (a). Therefore, the parameter for collective trim schedule was changed from the measured airspeed to the airspeed command of the IP which has rate limiter. The other cause of this issue was the low value of the proportional gain in the rotor speed feedback. The gain was scheduled to be reduced in airplane mode in order to avoid the speed sensitivity which is caused by the active collective command (θ_{0G}) of the rotor governor [12].

The final rotor speed overshoot was reduced to under ±0.5% RPM at the same airspeed region as shown in Fig. 9 (b). Note that Fig. 9 (b) shows higher airspeed command to match the airspeed with Fig. 9 (a) after calibration of aerodynamic lift coefficient.
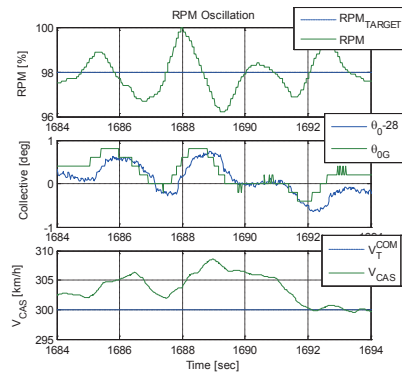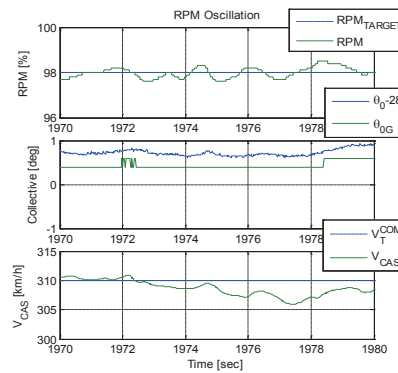

(a) Dynamic pressure correction
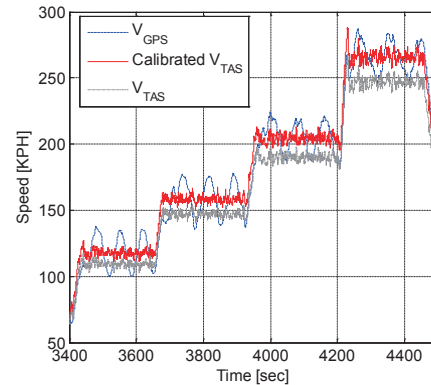
(b) Calibration results of true airspeed (V_{TAS})

Fig. 8. Calibration results of true air speed

(a) Large rotor speed oscillation

(b) Improved rotor speed oscillation

Fig. 9. Rotor speed oscillation in airplane mode

128

3.3.2 Slightly Low Damping in Roll Axis

The last anomaly of TR-100 was its slightly low damping in the roll axis under a high speed in airplane mode as shown in Fig. 10 (a). This tendency is similar to that of the TR-40, the 40% scaled model which showed low damping in the roll axis of airplane mode. The aerodynamic model yielded an over estimated rolling moment parameter against roll rate (L_p), so that the control gains were updated based on the parameter identification. The resultant damping in roll axis was improved as shown in Fig. 10 (b). The related stability margin of the both original and modified roll axis SCAS model are shown in Fig. 10 (c) and (d). The original gain margin is 9.25dB and the phase margin is 56.6deg. as shown in Fig. 10 (c). These margins were reduced to the minimum requirement of 6dB and 45deg. at the modified model in order to increase the roll damping by increasing roll axis feedback gains as shown in Fig. 10 (d). This means that the Smart UAV could meet the handing quality requirements in all flight envelopes with enough stability margins. Based on this experience, the control gains of the other variants of the tilt-rotor aircraft are designed to have optimized minimum gain margin ($\geq$ 6 dB) and phase margin ($\geq$ 45 deg.) [16].
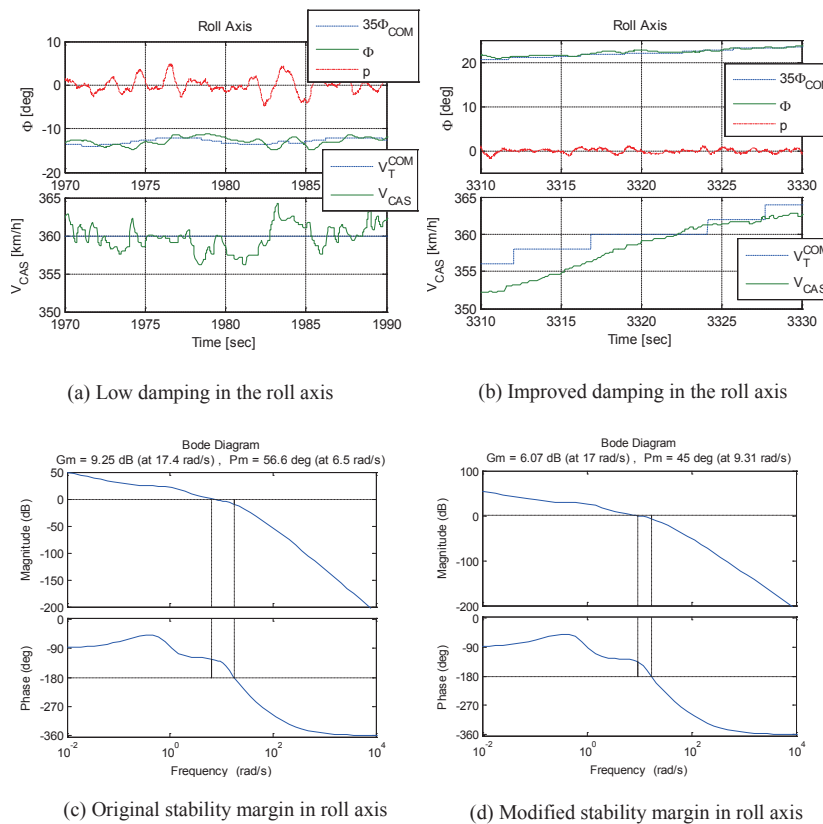
3.4 Comparison with Flight Envelop of Eagle Eye

The full flight envelope for the maximum speed sortie of the Smart UAV is compared with that of the TR-911X Eagle Eye in Fig. 11 [2, 5]. Note that the flight trajectories of Eagle Eye are approximately regenerated according to the flight test data [5]. The maximum true airspeed of the flight
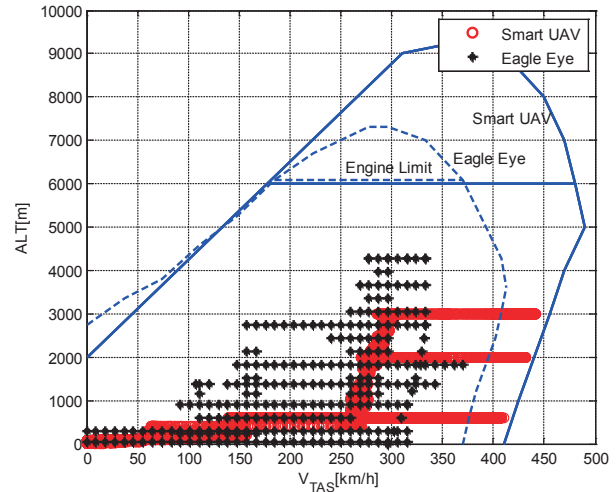

Fig. 11. Comparison of flight envelops of Smart UAV and Eagle Eye [2, 5]

(a) Low damping in the roll axis

(b) Improved damping in the roll axis

(c) Original stability margin in roll axis

(d) Modified stability margin in roll axis

Fig. 10. Damping of the roll axis in airplane mode

envelop of the Smart UAV is over 440km/h which is greater by an amount of over 70km/h at an altitude of 3km than that of the Eagle Eye, of which the maximum speed is 370km/h (i.e. 200kts). As the maximum altitude limit is dependent on the engine limit of Fig. 11, it is expected that both aircrafts yield similar levels of altitude performance, which could not be verified due to airspace limitation in Korea. However, the tested flight envelope shows that the Smart UAV is capable of reaching its maximum speed of over 480km/h at an altitude of 5km.

4. Conclusion

The flight test of the Smart UAV in helicopter, conversion, and airplane modes were completed. The Smart UAV accomplished a maximum speed of V_{TAS} 440km/h at an altitude of 3km [2]. Many unexpected problems that occurred during the envelope expansion positively contributed to improvement and led the Smart UAV to a better aircraft.

The stable and controllable characteristics of the control law of the Smart UAV were verified in all flight envelopes. In addition, it was shown that the vehicle was easy to handle for the IP without receiving assistance from the EP due to the full autonomous functions, which include take-off and landing. Therefore, the proven process of control law design could be applied to the family of tilt-rotor type UAVs in KARI [16].

The reliability of the newly developed FCS was evaluated under the dual redundancy and fault management system. All the faults that occurred during the flight test were effectively isolated and successfully replaced with the normal backup system. As a result, no fatal accident due to a single failure of the FCS system occurred during the flight tests. The production type of the DFCC will be integrated with the onboard ADC, resulting in the dual redundancy of the air data system for the dual DFCC.

The hardware in the loop simulation (HILS) and tethered hover test that followed the changes of the OFP contributed to the detection and filtering of many hidden software errors. The IP, EP, and the flight control engineers trained themselves during the HILS and changed the details of the flight plans to enable a safer and more effective test. The fidelity of the mathematical model used for the design of the control law was high enough to solve the flying quality problems during the flight test. The aerodynamic derivatives including C_L, C_D, and C_{lp} which showed some modeling error compared to the flight test results, were updated after the flight tests.

The Smart UAV program was completed successfully without any crash during the whole flight test, and the proven flight control technology is transferred to the new

production type of the tilt-rotor UAV, designated as the TR-60 which is scaled down to roughly 60% of the TR-100. It will be used for the military and civil missions of the Korean government.

New research topics of the tilt-rotor UAV will be conducted as follows: First, the research will focus on improving the range and endurance of the tilt-rotor UAV with the nacelle-mounted wing extension study [16].

Second, the ship deck operation capability will be investigated based on the HILS. The simulation will be conducted using the unsteady wake model around the ship that is generated by a computational fluid dynamics (CFD) tool.

Acknowledgement

References

[1] Kang, Y. S., Park, B. J., Cho, A., Yoo, C. S. and Koo, S. O., "Flight Test of Flight Control Performance for Airplane Mode of Smart UAV", *12th Conference of International Conference on Control Automation and Systems*, Jeju Island, Korea, 19 Oct., 2012., pp.1738-1741.

[2] Kang, Y. S., Park, B. J., Cho, A. Yoo, C. S. and Koo, S. O., "Analysis of Flight Test Result for Control Performance of Smart UAV", *Aerospace Engineering and Technology*, KARI, ISSN 1598-4168, Vol.12, No.1, July 2013, pp. 22-31.

[3] Ahn, O.S., "Advanced VTOL Concept for Smart UAV Program", *Nagoya-KyungSang Aero-Conference*, 2003.

[4] Fortenbaugh, R. L., Builta, K. E., Schulte, K. J., "Development and Testing of Flying Qualities for Manual Operation of a Tiltorotor UAV", *51st Annual Forum of American Helicopter Society*, Fort Worth, TX, USA, May 9-11, 1995., pp.299-320.

[5] Settle, B. and Wise, T. "Bell Eagle Eye TR–911X – Tiltrotor Unmanned Aerial Vehicle: Recent Developments, Autoland Integration, and Flight Test Demonstrations", *56th Annual Forum of American Helicopter Society*. Virginia, USA, May 2-4, 2000, pp. 306-319.

[6] Wyatt, D., Eagle Eye Pocket Guide, Bell Helicopter

Textron Inc., 2004.

[7] Schareffer, J. Alwang, R. and Joglekar, M. "V-22 thrust power management control law development", *47th Annual Forum of the American Helicopter Society*, Phoenix, Arizona, USA, 1991, pp. 1093-1100.

[8] Fortenbaugh, R., Hopkins, R. II and King, D., "BA609 First Flight VSTOL Handling Qualities," *60th Annual Forum of the American Helicopter Society*, Baltimore, MD, USA, June 7-10, 2004, pp.800-815.

[9] Choi, S.W., Kang, Y.S., Chang, S.H., Koo, S.O., Kim, J.M., "Development and Conversion Flight Test of a Small Tilt-rotor Unmanned Aerial Vehicle", *Journal of Aircraft*, Vol. 47, No.2, 2010, pp. 730-731.

[10] Kang, Y. S., Park, B. J., Yoo, C. S., Kim, Y. S. and Koo, S. O., "Fully Automatic Flight Test of Small Scaled Tilt Rotor Aircraft", *2nd International Forum on Rotorcraft Multidisciplinary Technology*, FP03-1, Oct. 19-20. 2009. pp. 31-34.

[11] Kang, Y. S., Park, B. J., Yoo, C. S., Koo, S.O. and Lee, J. H."Trouble Shooting for Fully Automatic Flight Test of Small Scaled Tiltrotor UAV", *Aerospace Engineering and Technology*, KARI, ISSN 1598-4168, Vol.8 No.1, 2009. pp. 1-9.

[12] Harendra, P.B., Joglkar, M.J., Gafey, T.M., Marr, R.L., *V/STOL Tilt Rotor Study - A Mathematical Model for Real Time Flight Simulation of The Bell 301 Tilt Rotor Research Aircraft*, NASA-CR-114614, NASA, April 1973.

[13] Yoo, C. S., Choi, H. S., Park, B. J., Ahn, S. J., Kang, Y. S., "Development of Simulation Program for Tilt Rotor Aircraft", *Journal of Institute of Control, Robotics and Systems*, Republic of Korea, Vol. 11, No. 3, March 2005., pp. 193-199.

[14] Kang, Y. S., Park, B. J., Cho, A., Yoo, C. S., Koo, S. O., "Trouble Shooting of Anomalies during Flight Test of Smart UAV", *The Korean Society for Aeronautical & Space Sciences (KSAS) conference*, TA4-1, 11 April 2013.

[15] Yoo, C. S., Ryu, S. D., Park, B. J., Kang, Y. S. and Jung, S. B., "Actuator Controller Based on Fuzzy Sliding Mode Control of Tilt Rotor Unmanned Aerial Vehicle", *International Journal of Control, Automation and Systems*, May 29 2014 (accepted for publication).

[16] Kang, Y.S., Park, B.J., Cho, A., Yoo, C.S., "Control Law Design for the Tilt-rotor Unmanned Aerial Vehicle with Nacelle Mounted Wing Extension (WE)", *Journal of Institute of Control, Robotics and Systems*, 2014., Vol.20, No.11, pp. 1103-1111.

[17] Kang, Y. S., Park, B. J., Cho, A., Yoo, C. S. and Koo, S. O., "Guidance Flight Test for Helicopter Mode of Smart UAV", *The Korean Society for Aeronautical & Space Sciences (KSAS) Conference*, FC2-3, 11 Nov. 2011, pp. 248-251.

[18] Kang, Y. S., Park, B. J., Cho, A., Yoo, C. S. and Koo, S. O., "Automatic Flight Test to Reduce Test Risk of Smart UAV in Helicopter, Conversion, and Airplane Mode", *1st Asia-Pacific International Symposium on Aerospace Technology*, FC-I-7.5.1., Jeju Korea., Nov. 2012.

[19] Park, B. J., Kang, Y. S., Cho, A., Chang, S. H. and Yoo, C. S., "Development of HILS System for Camera Guidance Mode Test of Smart UAV", *The Korean Society for Aeronautical & Space Sciences (KSAS) conference*, FG3-2, 11 April 2012. pp.500-505 .

[20] Park, B. J., Yoo, C. S., Cho, A., Kang, Y. S. and Koo, S. O., "Development of HILS System for Collision Avoidance Test of Smart UAV", *The Korean Society for Aeronautical & Space Sciences (KSAS) conference*, TB5-5, 11 Nov 2012. pp. 715-720.

[21] Fossen, T.I., *Marine Control Systems – Guidance, Navigation and Control of Ships, Rigs and Underwater Vehicles*. Marine Cybernetics (http://www.marinecybernetics.com), 2002, Norway, pp. 167-169.

[22] https://en.wikipedia.org/wiki/Undulation_of_the_geoid

[23] Kang, Y. S., Choi, S. W., Hwang, S. J., Ahn, O. S., Koo, S. O., Kim, J. M., "KARI Tiltrotor UAV Flight Test and Performance Enhancement Study", *38th European Rotorcraft Forum*, UAS-082, Amsterdam, Netherland, 4-7 Sep 2012.

[24] Wayne M. O., *Aircraft Performance Flight Testing, AFFTC-TIH-99-01*, Technical Information Handbook, A, Sep. 2000., pp. 31-32.

[25] Cho, A., Kang, Y. S., Park, B. J., Yoo, C. S., Koo, S. O., "Air data System Calibration Using GPS Velocity information", *12th International Conference on Control, Automation and Systems in ICC*, Jeju Island, Korea, Oct. 17-21, 2012.